Bidirectional Constant Current String-to-Cell Battery Equalizer Based on L2C3 Resonant Topology

Zhengqi Wei, *Student Member, IEEE*, Haoyu Wang, *Senior Member, IEEE*, Yiqing Lu, Dongdong Shu, Guangdong Ning, and Minfan Fu, *Senior Member, IEEE*

***Abstract*—In battery equalization systems, equalization speed, control complexity, and length of energy flow path are the important figures of merits. This article presents a novel bidirectional L2C3 resonant converter in a unique equalizer architecture with constant balancing current and fixed frequency control. The constant balancing current can be customized to achieve a stable balancing speed. The common equalizer unit transfers power bidirectionally between the entire string and any single cell. Design considerations of L2C3-based bidirectional equalizer are analyzed in detail, which ensures zero-voltage switching among all MOSFETS during the equalization process. The circuit is designed with synchronous rectification using the first harmonics approximation. The key contributions of this article include: a new bidirectional resonant topology for battery equalization; bidirectional constant current balancing with open-loop control; simplified synchronous rectification. An equalizer prototype with four lithium-ion battery cells at a balancing current of 500 mA is built and tested. The L2C3 circuit operates at 200 kHz with a peak efficiency of 89.4% and 90.1% under two balancing modes. Experimental results show the proposed scheme exhibits outstanding balancing performance.**

***Index Terms*—Battery equalizers, battery management system (BMS), electric vehicles (EVs), L2C3 converter, zero-voltage switching (ZVS).**

I. Introduction

PLUG-IN electric vehicles (PEVs) are booming and deemed the most promising solution to revolutionize transportation systems. Lithium-ion rechargeable battery plays the dominant role in traction battery in PEVs [1]. However, the terminal voltage of a single lithium-ion cell is low and limited in the range of 2.4–4.2 V [2]. Therefore, to meet the high power requirement of PEV, lithium-ion batteries are usually connected in series [3]. Due to the variations of manufaction, environment, and usage, such a battery pack usually encounters charge imbalance among cells [4]. This may lead to low available capacity, short lifetime, and a high risk of depletion and overcharge for the battery string [5]. Therefore, battery equalizers are necessary to effectively mitigate cell mismatch issues, and to improve the battery pack performance [6], [7], [8].

Power electronics intensive active balancing solutions can effectively mitigate cell mismatch with high energy efficiency [9]. Existing active balancing methods are mainly divided into five categories: cell-to-cell (C2C) [10], [11], [12], cell-to-buffer (C2B) [13], [14], [15], hierarchical module equalizer (HME) [16], [17], [18], cell-to-string (C2S) [19], [20], [21], and string-to-cell (S2C) [22], [23], [24].

Among them, conventional C2C method transfers charge between two battery cells. This method is introduced by using a common storage component, such as capacitor, inductor, or multiwinding transformer. However, its equalization speed is usually slow because the voltage gap of two cells is low [25]. C2B method utilizes a low-voltage auxiliary power supply as the energy buffer. A lead-acid battery is utilized to temporarily store energy from high-voltage cells and to charge low-voltage cells [26]. However, the auxiliary power supply is much smaller than the lithium battery pack, and its major task is to power the auxiliary loads. Hence, the equalization capacity of the lead-acid battery is limited. HME usually divides the battery pack into several submodules to realize the balance between modules and within submodules. It realizes a flexible charge flow. However, the multilevel structure requires complex control algorithms [27].

S2C structure can obtain a high balancing current due to the large voltage differences between the string and unbalanced cells [28]. Thus, these structures are suitable in scenarios with the voltage of a single cell lower than the average voltage of the cell string. In [24], a multiwinding transformer-based equalizer is proposed. It utilizes integrated rectifiers to reduce the count of active components. However, the bridge rectifiers limit the balancing direction. Each cell requires a dedicated transformer winding, which increases the transformer volume and degrades the efficiency. In [29], a half-bridge-converter-based equalizer, which reduces the switch count and achieves a high balancing current is proposed. However, one cell needs two inductors to suppress the current ripple. The equalizer suffers from bulky magnetics when the number of cells scales up. Nevertheless,

Manuscript received 18 July 2022; accepted 5 September 2022. Date of publication 9 September 2022; date of current version 10 October 2022. This work was supported in part by the National Natural Science Foundation of China under Grant 52077140 and in part by the Shanghai Rising Star Program under Grant 20QA1406700. Recommended for publication by Associate Editor S. A. Khajehoddin. *(Corresponding author: Haoyu Wang.)*

Zhengqi Wei is with the Center for Intelligent Power and Energy Systems, School of Information Science and Technology, ShanghaiTech University, Shanghai 201210, China, and also with the Department of Electrical Engineering, City University of Hong Kong, Kowloon Tong, Hong Kong (e-mail: weizhq1@shanghaitech.edu.cn).

Haoyu Wang, Yiqing Lu, Dongdong Shu, Guangdong Ning, and Minfan Fu are with the Center for Intelligent Power and Energy Systems, School of Information Science and Technology, ShanghaiTech University, Shanghai 201210, China (e-mail: wanghy@shanghaitech.edu.cn; luyq1@shanghaitech.edu.cn; shudd@shanghaitech.edu.cn; ninggd@shanghaitech.edu.cn; fumf@shanghaitech.edu.cn).

Color versions of one or more figures in this article are available at https://doi.org/10.1109/TPEL.2022.3205440.

Digital Object Identifier 10.1109/TPEL.2022.3205440

when the voltage of one cell reaches the upper threshold, charge needs to be transferred to the cells, which are not fully charged. C2S structures require the least balancing cycles under this scenario. Normal S2C balancing structures become complex and multiple balancing cycles are needed since the charge flow is unidirectional. More seriously, the cells that need to be charged and discharged are usually in the same battery string. This means more balancing cycles of both S2C and C2S are inevitable.

Some bidirectional equalizers are proposed to realize S2C and C2S balancing. Qi et al. [30] proposed an integrated cascade structure, which is equivalent to the cascade of a bidirectional buck-boost converter and a bidirectional bridge converter. This method achieves a high voltage conversion ratio with a low transformer turn ratio. However, the control complexity of the cascade system is high. Thus, the robustness is unsatisfactory. Lu et al. [31] proposed a quasiresonant bidirectional equalizer, which can achieve ZVS in both boost and buck modes through a quasiresonance operation. However, it can be observed that its efficiency performance and components count is unsatisfactory. Uno et al. [32] proposed a modular equalizer based on a DPS-controlled capacitively-isolated-dual-active-bridge converter, which uses a multilevel structure to achieve a flexible energy flow with low component count. This structure also reduces the voltage stress of MOSFETS, which is related to the number of modules. However, the charge can only be transferred between submodules, not inside modules, and the number of selection switches is high. Hannan et al. [31] proposed a bidirectional flyback converter-based equalizer, which is featured with low components count and low control complexity. However, this method has large current fluctuations, which cause an increase in the conduction loss.

To resolve these problems, this article proposes a novel equalizer based on a bidirectional L2C3 resonant converter. The attractive features include the following.

1) A novel bidirectional isolated converter is proposed, which is suitable for battery equalizer systems. The circuit is properly designed for the system, and the design methodology is analyzed and detailed.
2) The proposed bidirectional equalizer achieves bidirectional charge transfer between the entire cell string and any single cell. Therefore, compared with conventional S2C and C2S structures, this equalizer offers more flexible charge flow paths to reduce the balancing cycles.
3) Due to the output characteristic of L2C3 resonant topology, bidirectional constant balancing current can be achieved with open-loop control. Only a pair of complementary driving signals with fixed switching frequency is required. This simplifies the circuit design and reduces the control complexity.
4) All MOSFETS are turned-ON with ZVS and the implementation of the synchronous rectification can reduce the conduction loss.

The rest of this article is organized as follows. The balancing operation and control strategy of the L2C3-based equalizer architecture are introduced in Section II. Design methodology and balancing efficiency are given in Section III. Synchronous rectification in S2C and C2S mode is analyzed in Section IV.

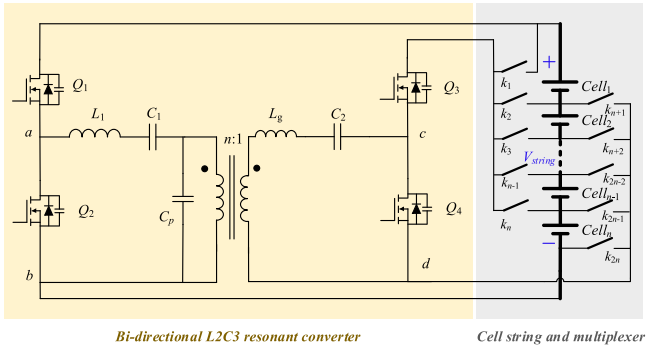

Fig. 1. Schematic of the proposed L2C3-based S2C equalizer.

Section V provides the design of the prototype and experimental results. Section VI compares various equalizers comprehensively. Finally, Section VII concludes this article.

II. Proposed Equalizer and Operation Principles

A. Operating Principles

The schematic of the proposed equalizer to balance four series-connected batteries is plotted in Fig. 1. As shown, it is based on a shared bidirectional L2C3 resonant converter. The constant current balancing between cell and battery string can be automatically obtained by driving the MOSFET switches using two pairs of complementary PWM signals with a fixed frequency and duty cycle. The transformer turns ratio (n) is 1, and the detailed analysis is performed in Section III. When the equalizer operates in S2C mode, Q_1 and Q_2 function as inverter, and Q_3 and Q_4 function as synchronous rectification. The battery string can be seen as input voltage source ($V_{\text{in,S2C}} = V_{\text{string}} = NV_{\text{Cell}}$), and the target cell is the load.

When the equalizer operates in C2S mode, the functions of the primary and secondary side switches are interchanged. The single cell whose voltage is higher than that of the other cells can be seen as input voltage source ($V_{\text{in,C2S}} = V_{\text{Cell}}$), and the cell string is the load.

B. Control Strategy of the Proposed Equalizer

The control flowchart is plotted in Fig. 2. As shown, the control unit measures the voltage of each cell and estimates the open circuit voltage (OCV). When OCV_n of one cell is lower than OCV_{nor} ($\text{OCV}_n < \text{OCV}_{\text{nor}}$), the system should work in S2C mode. For example, the selected cell is Cell_1, relay k_1 and k_{1+n} are turned-ON, where n is the number of cells in battery string. Then, the MOSFETS $Q_1 - Q_2$ and $Q_3 - Q_4$ are driven with 50% duty cycle in a complementary manner while the phase shift φ_1 between $Q_1 - Q_2$ and $Q_3 - Q_4$ is regulated to achieve synchronous rectification. Then, $\Delta\text{OCV}_{\text{S2C}}$ need to be calculated by

$$\Delta\text{OCV}_{\text{S2C}} = \text{OCV}_{\text{nor}} - \text{OCV}_{\text{min}} \tag{1}$$

where OCV_{nor} is the OCV of the normal cell. When the voltage mismatch is lower than 5 mV, equalization accuracy is reached, but the equalization needs to be extended for t_{S2C}. It is related

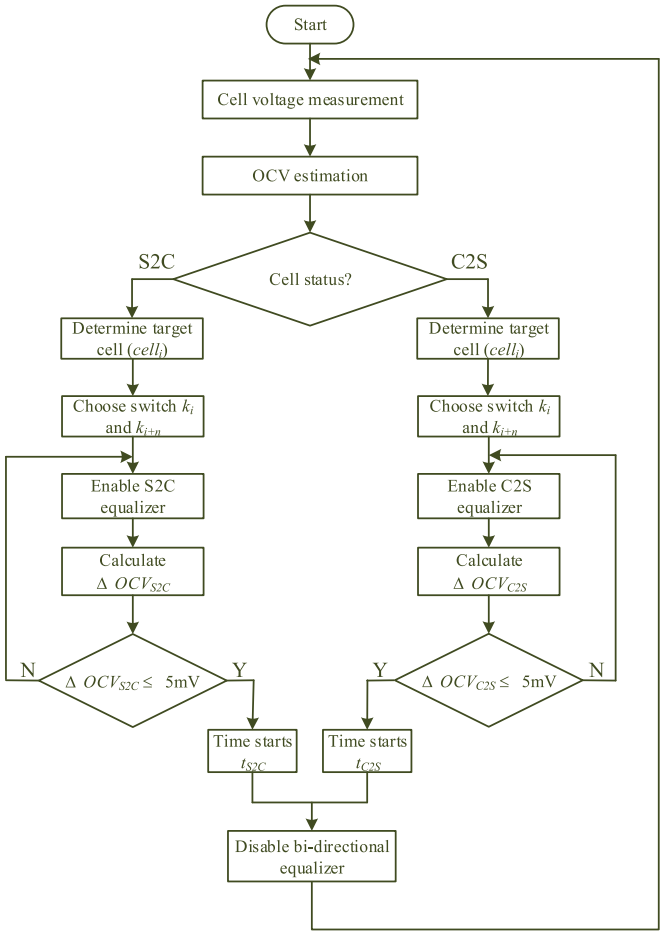

Fig. 2. Control strategy of the bidirectional equalization.

to the recovery effect of the battery. The calculation method of t_{S2C} is analyzed in detail in the [22].

Similarly, when OCV_n of one cell is higher than OCV_{nor} ($OCV_n > OCV_{nor}$), the system should work in C2S mode. ΔOCV_{C2S} can be calculated by

$$\Delta OCV_{C2S} = OCV_{max} - OCV_{nor}. \quad (2)$$

If the battery state in the battery string requires two equalization modes, the equalizer first operates in S2C mode and then switches to C2S mode.

C. S2C Mode

According to the control principle of charge equalization, when a single cell is undercharged, equalization is activated. In this case, charge is transferred from the battery string to the unbalanced cell, and the equalizer operates in the S2C mode. Fig. 3 demonstrates the corresponding key waveforms in one switching cycle in S2C mode. The operation of the equalization unit can be divided into six modes. Their equivalent circuits of four batteries are illustrated in Fig. 4. Each mode can be described briefly as follows.

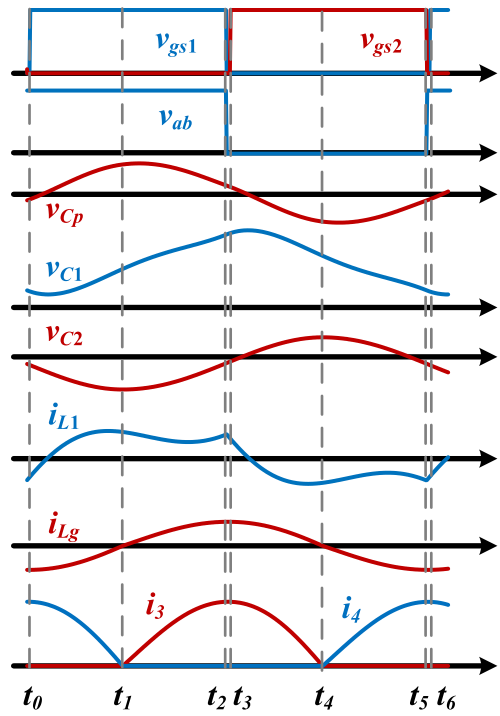

Fig. 3. Key steady-state waveforms in S2C mode.

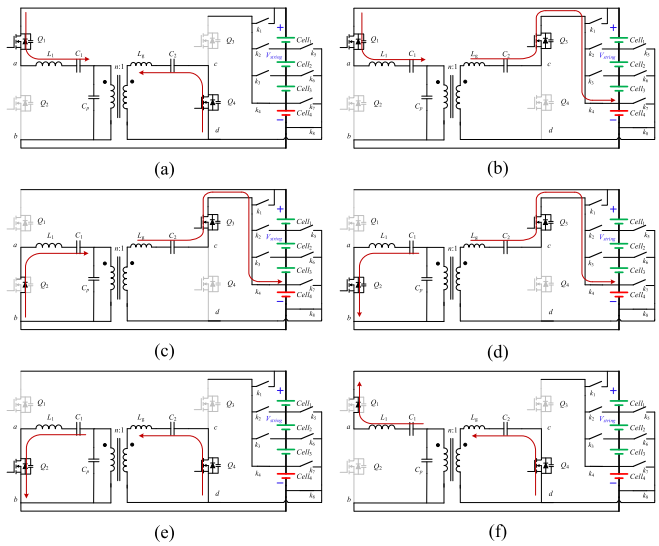

Fig. 4. Equalization equivalent circuits of an undercharged cell in S2C mode. (a) Mode 1 ($t_0 - t_1$]. (b) Mode 2 ($t_1 - t_2$]. (c) Mode 3 ($t_2 - t_3$]. (d) Mode 4 ($t_3 - t_4$]. (e) Mode 5 ($t_4 - t_5$]. (f) Mode 6 ($t_5 - t_6$].

Mode I, $t \in [t_0, t_1)$, Q_1 is turned-ON with ZVS, and Q_2 remains OFF. In this mode, i_{L1} does not return to zero, and the resonant tank releases charge to the battery string through Q_1.

Mode II, $t \in [t_1, t_2)$, the body diode of Q_4 is reversely biased and the body diode of Q_3 conducts. Parallel resonant capacitor (C_p) begins to be discharged, the terminal voltage of C_p (V_{cp}) decreases.

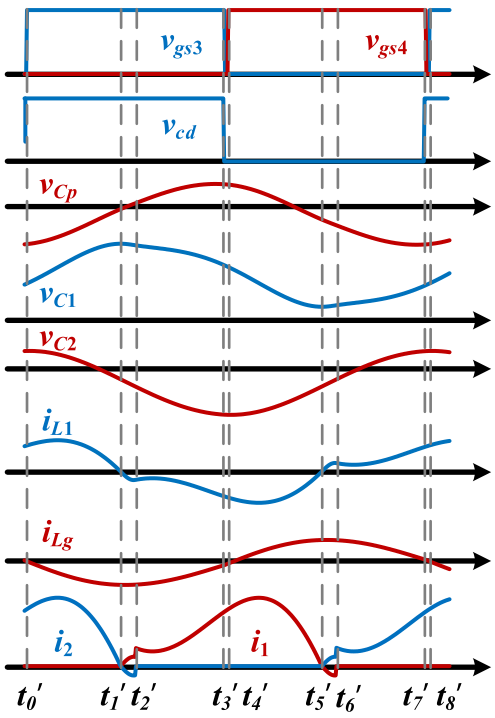

Fig. 5. Key steady-state waveforms in C2S mode.

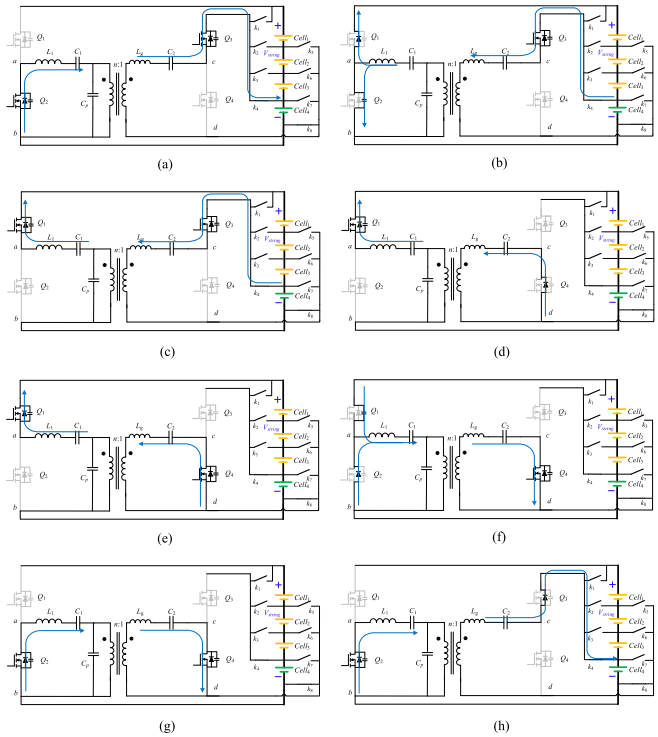

Fig. 6. Equalization equivalent circuits of an undercharged cell in C2S mode. (a) Mode 1 ($t_0' - t_1'$]. (b) Mode 2 ($t_1' - t_2'$]. (c) Mode 3 ($t_2' - t_3'$]. (d) Mode 4 ($t_3' - t_4'$]. (e) Mode 5 ($t_4' - t_5'$]. (f) Mode 6 ($t_5' - t_6'$]. (g) Mode 7 ($t_6' - t_7'$]. (h) Mode 8 ($t_7' - t_8'$].

Mode III, $t \in [t_2, t_3)$, Q_1 is turned-OFF. C_{oss1} starts to be charged, while C_{oss2} starts to be discharged. During the dead band, i_{Lr} commutates to Q_2 and flows through its body diode. This means that the body diode conducts before Q_2 turns-ON, which creates a ZVS condition for Q_2.

From t_3, the resonant converter enters the second half cycle, which is similar to the first half cycle.

D. C2S Mode

When a single cell is detected to be in an overcharged state, the extra energy is transferred from the overcharged cell to the battery string. In this case, the proposed equalizer operates in C2S mode. According to the operating waveforms shown in Fig. 5, the converter has eight stages in one switching cycle in the C2S mode. Fig. 6 shows the specific working process.

Mode I, $t \in [t_0', t_1')$, the negative i_{Lg} discharges and charges the output capacitance C_{oss} of Q_3 and Q_4, respectively. Thus, Q_3 is turned-ON with ZVS. At this instant, i_{Lg} returns to zero, and the direction of i_{Lg} is to the right.

Mode II, $t \in [t_1', t_2')$, Q_3 remains ON. The parallel resonant capacitor C_p is charged, and C_{oss2} resonate with L_1. Meanwhile, the body diode of Q_1 conducts.

Mode III, $t \in [t_2', t_3')$, i_{Lg} decreases and Q_3 remains ON. In this mode, Q_1 is turned-ON with ZVS, and synchronous rectification is activated.

Mode IV, $t \in [t_3', t_4')$, Q_3 is turned-OFF, C_{oss3} starts to be charged, while C_{oss4} starts to be discharged. During the dead band, i_{Lg} commutates to Q_4 and flows through its body diode,

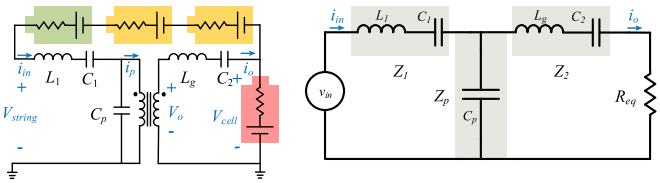

Fig. 7. Equivalent circuit when Cell_4 is underbalanced.

which means that the body diode conducts before Q_4 turns-ON. This creates the ZVS condition for Q_4.

From t_4', the resonant converter enters the second half cycle, which is similar to the first half cycle.

III. Design Considerations

A. Current Gain

First harmonics approximation (FHA) method is used to analyze the circuit [33], [34], [35]. Fig. 7 shows the simplified equivalent circuit of L2C3 resonant converter. Because the analysis of two modes is identical, only S2C mode is analyzed as an example. The current gain of the resonant converter is shown as

$$G_I = \frac{i_o}{v_{\text{in}}} = \frac{1}{(Z_2 + R_{\text{eq}})//Z_p + Z_1} \cdot \frac{Z_p}{Z_p + Z_2 + R_{\text{eq}}}. \quad (3)$$

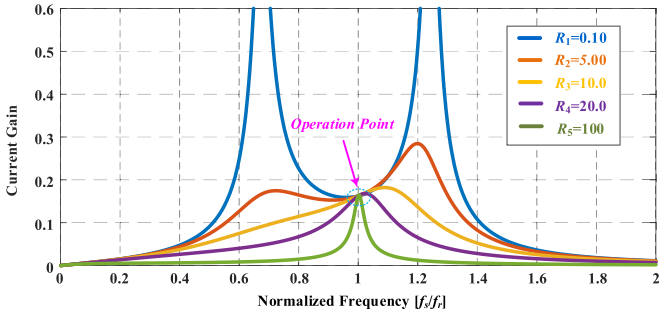

Fig. 8. Current gain curves versus normalized f_n.

The impedance of each element of the resonant tank can be expressed as

$$\begin{cases} Z_1 &= j\omega_s L_1 + \frac{1}{j\omega_s C_1} \\ Z_2 &= j\omega_s L_g + \frac{1}{j\omega_s C_2} \\ Z_p &= \frac{1}{j\omega_s C_p}. \end{cases} \tag{4}$$

According to (1) and (2), the current gain of the resonant converter can be derived as (3), where ω_s is angular switching frequency.(5) shown at bottom of this page, According to (3), the current gain is independent of load when the (4) is satified

$$\omega_s L_1 - \frac{1}{\omega_s C_1} - \frac{1}{\omega_s C_p} = 0 \tag{6}$$

$$\omega_s = \omega_r = \frac{1}{\sqrt{L_1 \frac{C_1 C_p}{C_1 + C_p}}}. \tag{7}$$

The curves of current gain versus normalized frequency under different load conditions are depicted in Fig. 8. As shown, the curves converge at $f_n = f_s/f_r = 1$. Thus, when the converter is designed to operate near the resonant frequency, in the balancing process, the range of balancing current change caused by the change of equivalent load is trivial.

B. Parameters Design

To design the resonant tank, there are six parameters to be identified. They are resonant inductance L_1, leakage inductance L_g, resonant capacitances C_1, C_2, and C_p, and transformer turns ratio n. Symmetrical design is expected, which helps reduce the design complexity. In addition, conduction loss is the dominant power loss. Thus, to improve the efficiency of both balancing modes (S2C and C2S), n is set to 1.

1) Resonant Inductance (L_1) and Leakage Inductance (L_g): To minimize the switching loss, all MOSFETS should be turned-ON with ZVS. Therefore, the resonant parameters design should be considered. The imaginary part of Z_{in} can be expressed as

$$b_1 = L_1\omega_s - \frac{1}{C_1\omega_s} + \frac{(C_2 L_g \omega_s^2 - 1)(-C_2 C_p L_g \omega_s^2 + C_2 + C_p)}{\omega_s \sigma_1}$$

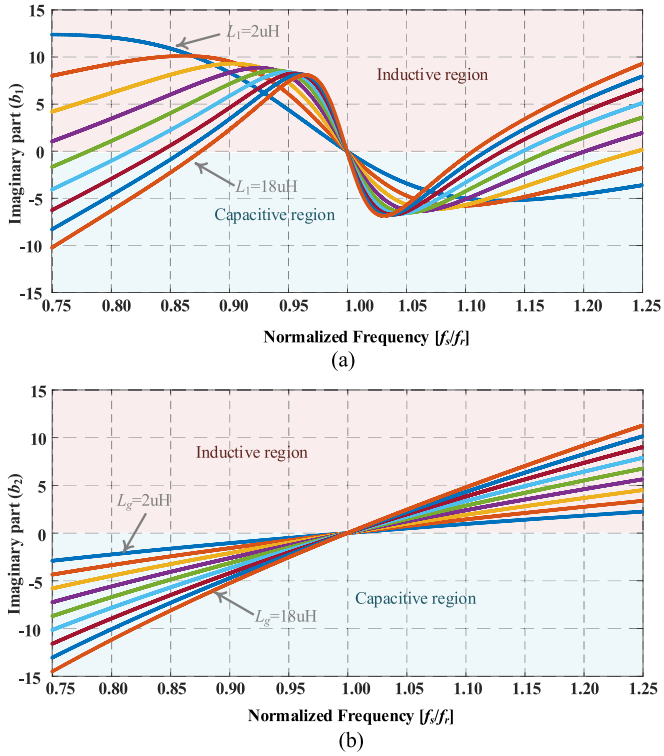

Fig. 9. (a) Imaginary parts of resonant tank impedance (b_1) versus normalized frequency f_n. (b) Imaginary parts of resonant tank impedance (b_2) versus normalized frequency f_n.

$$- \frac{C_2 C_p R_{\text{eq}} \omega_s^2}{\sigma_1} \tag{8}$$

where

$$\sigma_1 = \left(-C_2 C_p L_g \omega_s^2 + C_2 + C_p\right)^2 + {C_2}^2 {C_p}^2 R_{\text{eq}}^2 \omega_s^2. \tag{9}$$

Meanwhile, the equations of C2S balancing process can be derived similarly. The imaginary parts of resonant tank impedance (b_1 and b_2) of S2C and C2S are plotted in Fig. 9. As shown in Fig. 9(a), when f_s is lower than f_r, the MOSFETS (Q_1 and Q_2) turn-ON with ZVS. As shown in Fig. 9(b), when f_s is higher than f_r, the MOSFETS (Q_3 and Q_4) turn-ON with ZVS. However, f_s needs to be close to f_r to maintain a constant balancing current in the equalization process. Meanwhile, the inductance cannot be too large since the current gain varies sharply with the increase of series inductance. This leads to a significant attenuation of equalization current. Therefore, series resonant inductance (L_1) and leakage inductance (L_g) should be designed between 7 and $8\mu H$, which affects current gain and ZVS condition.

2) Resonant Capacitances (C_p and $C_{1,2}$): According to the equivalent circuit of equalizer, the fundamental component of v_{ab} (v_{ab1}) is expressed as

$$v_{ab1} = v_{\text{in}} = \frac{2V_{\text{String}}}{\pi} \sin(\omega_s t). \tag{10}$$

$$G_I = \frac{1}{\omega_s C_p \left[\left(-\omega_s L_1 + \frac{1}{\omega_s C_1} + \frac{1}{\omega_s C_p}\right) R_{eq} + j\left(\frac{L_1}{C_p} - \frac{1}{C_1 C_p \omega_s^2} + \frac{L_g}{C_p} - \frac{1}{C_2 C_p \omega_s^2} - \omega_s^2 L_1 L_g + \frac{L_g}{C_1} + \frac{L_1}{C_2} - \frac{1}{\omega_s^2 C_1 C_2}\right)\right]} \tag{5}$$

The output current i_{eq1} is expressed as

$$i_{\text{eq1}} = \frac{\pi I_o}{n} \sin(\omega_s t + \theta). \tag{11}$$

Thus, combining with (8) and (9), the resonant parallel capacitance can be derived as

$$C_p = \frac{\pi I_o}{4nV_{\text{string}} f_s}. \tag{12}$$

Resonant angular frequency of L2C3 converter can be shown as

$$\omega_r = \sqrt{\frac{C_1 + C_p}{L_1 C_1 C_p}}. \tag{13}$$

Combining (10) and (11), the series capacitance can be expressed as

$$C_1 = C_2 = \frac{C_p}{\omega_r^2 L_1 C_p - 1}. \tag{14}$$

C. Balancing Power and Efficiency

Power is transferred from the primary side (cell string) to the secondary side (single cell) in S2C mode and it flows back to the cell string from single in C2S mode. The converter can be seen as a constant current source. Therefore, the balancing current can be maintained at the design value, while the change of battery voltage can be regarded as approximately linear. The balancing power in S2C mode can be calculated as

$$P_{b,\text{S2C}} = \frac{V_{\text{Cell}} + V_{\text{end}}}{2} I_{o,\text{S2C}} \tag{15}$$

where V_{end} is the cell voltage after equalization.

In C2S mode, the cell string is connected to the output side. The balancing power in C2S mode can be calculated as

$$P_{b,\text{C2S}} = \frac{4V_{\text{end}} + \sum_{n=1}^{4} V_{\text{Cell}}}{2} I_{o,\text{C2S}}. \tag{16}$$

The design value of the balancing current is 500 mA, and the cell and string voltage is 3.65–3.75 V and 15.15–15.20 V, respectively. Therefore, when the system equalizes one battery cell, the transferred power is about 1.85 W in S2C mode and 1.90 W in C2S mode.

The loss calculation method of the converter in the two equalization modes is the same, so we take S2C as an example. The balancing loss mainly consists of four parts, the switching loss, transformer loss, inductor loss, and capacitor loss.

1) Switching Loss: The proposed equalizer can achieve ZVS turn-ON. Thus, the turn-ON loss of MOSFET is negligible, the switching loss mainly attributes to the MOSFET turn-OFF loss. and conduction loss. The turn-OFF loss of the MOSFETS of primary side and secondary side can be expressed as, respectively

$$P_{\text{off},p} = \left(\frac{1}{2} V_{\text{String}} I_{\text{off}} T_{\text{off}} - \frac{1}{2} C_{\text{oss}} V_{\text{String}}^2\right) f_s$$

$$P_{\text{off},s} = \left(\frac{1}{2} V_{\text{Cell}} I_{\text{off}} T_{\text{off}} - \frac{1}{2} C_{\text{oss}} V_{\text{Cell}}^2\right) f_s$$

where I_{off} is the MOSFET current at the turn-OFF. T_{off} is the turn-OFF time and can be estimated from the datasheet. The conduction loss of MOSFETS S_1–S_4 can be expressed as

$$P_{\text{con}} = R_{\text{on}} I_{\text{rms}}^2$$

where R_{on} is the on resistance of MOSFETS, and I_{rms} is the rms current of resonant tank. Therefore, the switching loss can be shown as

$$P_{\text{sw}} = P_{\text{off},p} + P_{\text{off},s} + 2P_{\text{con}}.$$

2) Transformer Loss: The transformer loss includes core loss and coil loss. Steinmetz's equation is used to estimate the core loss

$$P_{\text{core}} = K_c f_s^{\alpha} \Delta B^{\beta}$$

where K_c, α, and β are provided from the datasheet and ΔB is the variation of the magnetic flux of the balancing transformer, and it can be calculated based on the Faraday law of electromagnetic induction. The coil loss of equalization transformer (P_{coil}) is a part of conduction loss. It can be calculated as follows:

$$P_{\text{coil}} = \rho_w \frac{l_w}{A_w} I_{\text{rms}}^2$$

where, ρ_w, l_w, and A_w are the parameters of the conductors and I_{rms} is the rms current. It should be noted that Litz wire and interleaved winding help to mitigate the skin effect and proximity effect. Thus, the transformer loss can be calculated as follows:

$$P_{\text{trans}} = P_{\text{core}} + P_{\text{coil}}.$$

3) Inductor Loss: The calculation method of series connected inductor loss is the same as that of transformer. Only one extra inductor (L_1) on the primary side is added. Thus, the inductor loss can be calculated as follows:

$$P_{L1} = P_{L\_\text{core}} + P_{L\_\text{coil}}.$$

4) Capacitor Loss: The capacitor loss can be calculated as follows:

$$P_C = \text{ESR} \cdot I_{\text{rms}}^2$$

where ESR was measured experimentally. Since the turns ratio of transformer, the power loss of C_1 is equal to C_2. Rms current value of parallel and series connected capacitor can be calculated by simulation.

IV. Synchronous Rectification Analysis

Synchronous rectification can improve the efficiency during the balancing process due to less voltage drop on the MOSFET channel than the body diode [36]. This section analyzes the SR method in S2C mode and C2S mode.

Fig. 10(a) demonstrates the SR gating signals in the S2C mode. At t_1, i_{Lg} reaches zero and goes to positive. It charges C_{oss} of the MOSFET (Q_4) and discharges C_{oss} of the MOSFETS (Q_3). At t_2, body diodes of switch (Q_3) conduct. Therefore, Q_3 achieve ZVS turning-ON. At t_3, i_{Lg} reaches zero. Thus, MOSFET (Q_3) is turned-OFF with ZCS.

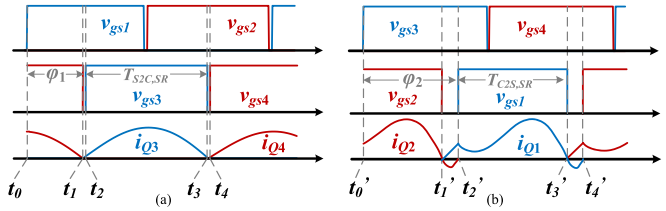

Fig. 10. SR waveforms. (a) S2C mode. (b) C2S mode.

Fig. 10(b) demonstrates the SR gating signals in C2S mode. During t_1'–t_2', L_1 resonates with C_{oss}. The body diode of Q_1 conduct, with a proper dead band, ZVS can be achieved in the half-bridge.

The half-bridge can be seen as voltage multiplier

$$v_{\text{cd1}} = \frac{2k_1 V_{\text{Cell}}}{\pi} \sin(\omega_s t) \tag{17}$$

where v_{cd1} is the fundamental frequency components of v_{cd}. $k_1 = \{1, 2, 3\}$ is the number of cells. When multiple adjacent cells are balanced in S2C mode, $k_1 > 1$

$$R_{\text{S2C,eq}} = \frac{k_1 V_{\text{Cell}}}{I_{\text{S2C},o}} \tag{18}$$

$$R_{\text{C2S,eq}} = \frac{V_{\text{string}}}{k_2 I_{\text{C2S},o}} \tag{19}$$

where $k_2 = \{1, 2, 3\}$ is the cell number in C2S mode. In this mode, the output current is proportional to the number of batteries at the input port. The primary-side and secondary-side equivalent ac load resistance ($R_{\text{C2S,ac}}$, $R_{\text{S2C,ac}}$) can be derived as

$$R_{\text{S2C,ac}} = \frac{2R_{\text{S2C,eq}}}{\pi^2} \tag{20}$$

$$R_{\text{C2S,ac}} = \frac{2R_{\text{C2S,eq}}}{\pi^2}. \tag{21}$$

FHA method is used to calculate the phase shift (φ)

$$\varphi_1 = \text{angle}\left(\frac{Z_p}{Z_p(Z_2+R_{\text{S2C,ac}})+Z_1Z_p+Z_1(Z_2+R_{\text{S2C,ac}})}\right) \tag{22}$$

$$\varphi_2 = \text{angle}\left(\frac{Z_p}{Z_p(Z_1+R_{\text{C2S,ac}})+Z_2Z_p+Z_2(Z_1+R_{\text{C2S,ac}})}\right). \tag{23}$$

The SR delay in S2C and C2S modes is as follows:

$$t_1 - t_0 = \frac{\varphi_1}{\omega_{s1}} = \frac{\varphi_1}{2\pi f_{s1}} \tag{24}$$

$$t_1' - t_0' = \frac{\varphi_2}{\omega_{s2}} = \frac{\varphi_2}{2\pi f_{s2}}. \tag{25}$$

In S2C mode, the duration of conduction time $T_{\text{S2C,SR}}$ in Q_3 and Q_4 is

$$T_{\text{S2C,SR}} = t_3 - t_2 = \frac{1}{2f_{s1}} - t_d. \tag{26}$$

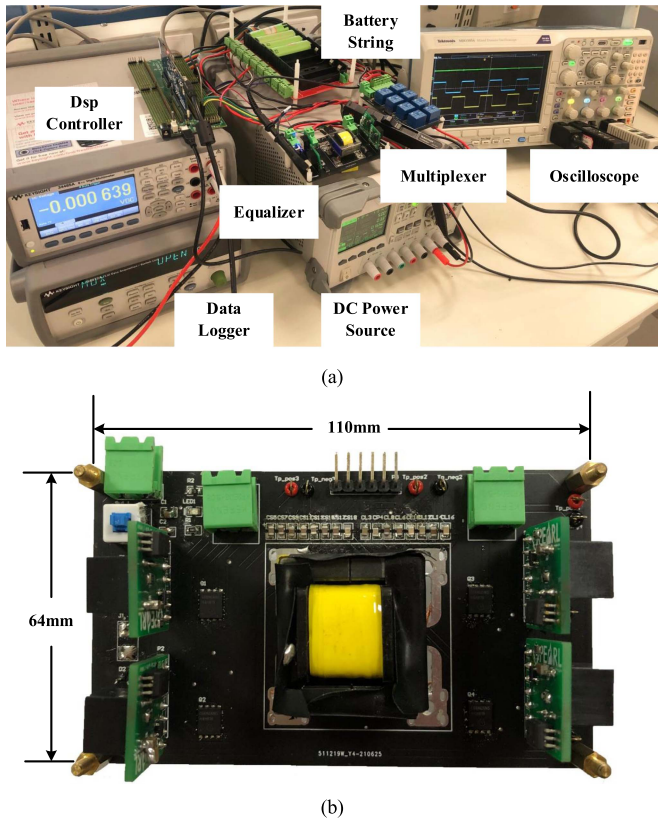

Fig. 11. (a) Experimental setup. (b) Designed bidirectional L2C3 equalizer prototype.

To achieve ZVS turning-ON, t_d is derived as

$$\frac{1}{\omega_{s1}}\{\arccos[f_{s1}C_{\text{oss}}|Z_{\text{S2C}}| + \cos(\varphi_1)] - \varphi_1\} \leqslant t_d \leqslant \frac{\varphi_1}{2\pi}T_s. \tag{27}$$

In C2S mode, the duration of conduction time $T_{\text{C2S,SR}}$ in Q_1 and Q_2 is

$$T_{\text{C2S,SR}} \leqslant t_3' - t_2' = \frac{1}{2f_{s2}} - t_d' \tag{28}$$

where t_d' can be regarded as half of the L_1 and C_{oss} resonance period. Therefore, t_d' can be derived as

$$t_d' = t_2' - t_1' = \pi\sqrt{2L_1C_{\text{oss}}}. \tag{29}$$

V. Experimental Results

In order to validate the analysis and design of the proposed bidirectional equalizer, as shown in Fig. 11, a prototype of four lithium-ion cells is implemented and tested. The circuit parameters are summarized in Table I. Four 2900 mAh Panasonic NCR18650PF lithium-ion cells are employed in the prototype. The module multiplex network is implemented by relays (SRD05VDC). Fig. 12(a) and (b) shows the key waveforms of S2C balancing and C2S balancing, respectively. It can be seen that all the MOSFETS are turned-ON with ZVS, which verifies the theoretical analysis. It can be observed that the balancing current under S2C mode with $f_s = 196.0\,\text{kHz}$ is 500 mA, and

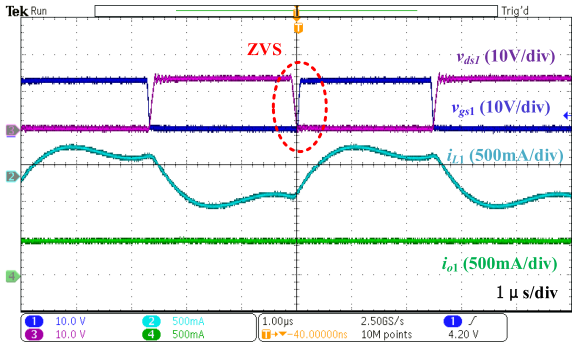

Fig. 12. Key waveforms of the L2C3-based bidirectional equalizer. (a) Gate drive signal $v_{\rm gs1}$, drain source voltage $v_{\rm ds1}$ of Q_1, inductor current i_{L_1}, and output current i_{o1} in S2C mode. (b) Gate drive signal $v_{\rm gs3}$, drain source voltage $v_{\rm ds3}$ of Q_3, leakage inductor current i_{L_g}, and output current i_{o2} in C2S mode.

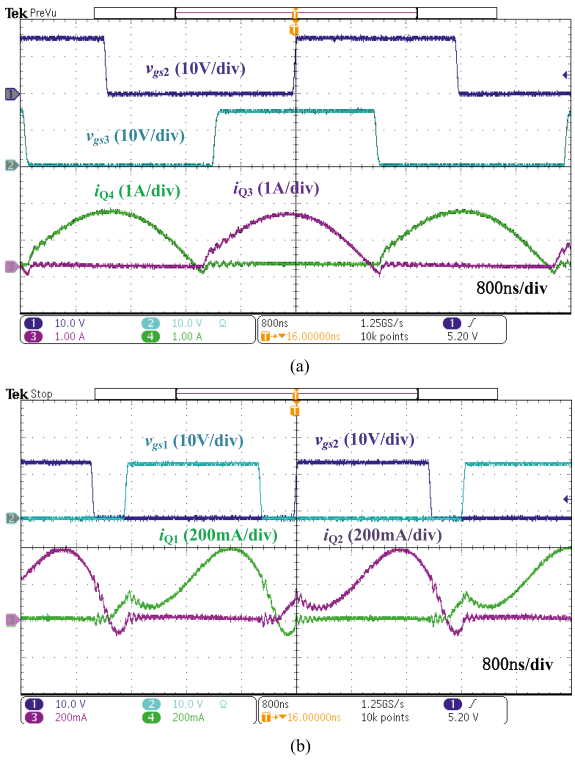

Fig. 13. Key waveforms of synchronous rectification. (a) Gate drive signal of primary side $v_{\rm gs2}$ of Q_2, gate drive signal of synchronous rectifier $v_{\rm gs3}$ of Q_3, Q_3 current i_{Q3}, and Q_4 current i_{Q4} in S2C mode. (b) Gate drive signal of synchronous rectifier $v_{\rm gs1}$ of Q_1, $v_{\rm gs2}$ of Q_2, Q_1 current i_{Q1}, and Q_2 current i_{Q2} in C2S mode.

TABLE I
CRITICAL DESIGN PARAMETERS

Component Type	Parameters
Microcontroller	TMS320F28379
MOSFET	BSC052N03LS
MOSFET driver	ACPL-W343
Relay	SRD-05VDC
Relay driver	TDB62083AFWG
Battery	NCR18650PF
S2C switching frequency(f_{s1})	196.0 kHz
C2S switching frequency(f_{s2})	204.1 kHz
Turns ratio(n)	12:12
Series inductor (L_1)	7.54 μH
Leakage inductor (L_g)	7.70 μH
Series capacitor (C_1)	235.01 nF
Series capacitor (C_2)	221.85 nF
Parallel capacitor (C_p)	130.9 nF

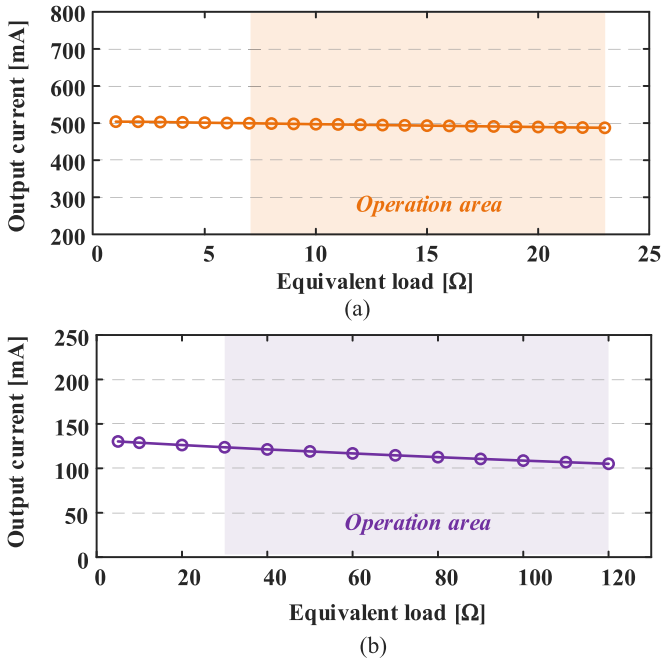

Fig. 14. Experimentally measured output current of the L2C3-based equalizer versus equivalent load. (a) S2C mode. (b) C2S mode.

the current under C2S mode with $f_s = 204.1$ kHz is 125 mA. Fig. 13 shows the experimental waveforms of the synchronous rectification.

As shown in Fig. 14(a), in S2C mode when the proposed equalizer output voltage is equal to the change of load in the actual process of single cell battery balancing, the output balancing current is 504 mA. When the load range is equal to three batteries, the output current varies from 504 to 487 mA. Fig. 14(b) shows the balancing current in C2S mode varies from 130 to 105 mA. These indicate that the proposed bidirectional equalizer exhibits a good open-loop constant current behavior.

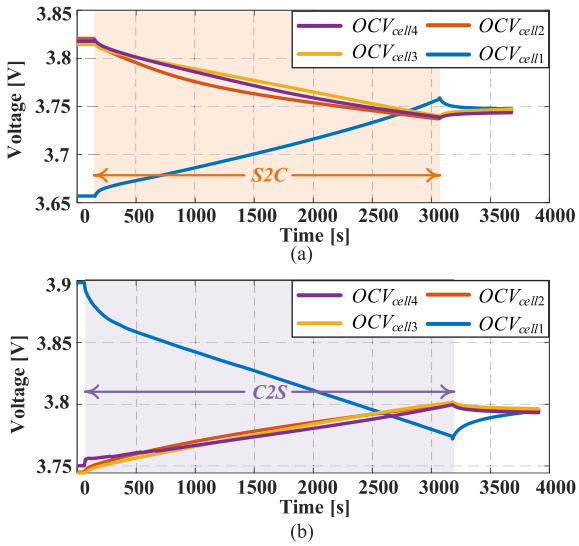

Fig. 15. Cell voltages during the equalization process with different balancing path. (a) S2C mode. (b) C2S mode.

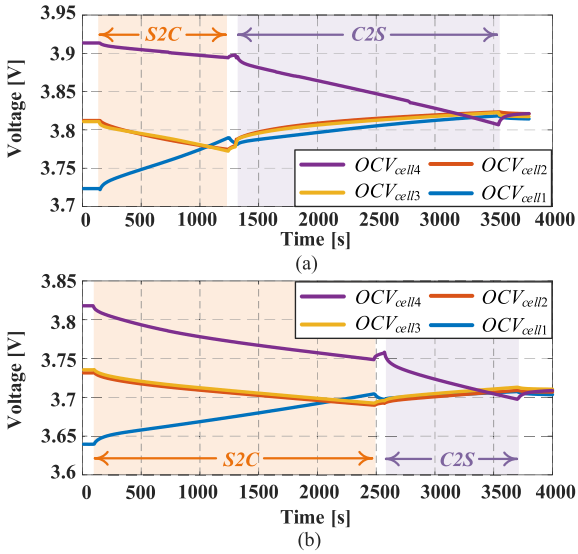

Fig. 16. Equalization results for four cells with different distributions. (a) Initial OCVs (OCV_{cell}) are 3.914, 3.814, 3.811, and 3.723 V. (b) Initial OCVs (OCV_{cell}) are 3.818, 3.735, 3.732, and 3.632 V.

Fig. 15(a) and (b) shows the experimental results for four battery cells. The voltage data are recorded by a data logger (Keysight 34972 A). As shown in Fig. 15(a), when the voltage of a certain battery is lower than the threshold voltage, the equalization circuit reduces the voltage difference from 151 to 7 mV in 2910 s. In Fig. 15(b), when the voltage of a certain battery is higher than the threshold voltage, the equalization circuit reduces the voltage difference from 158 to 6 mV in 3110 s.

In order to further verify the performance of the proposed bidirectional equalizer, the experimental results are captured in Fig. 16(a) and (b). The balancing process can be divided into two stages (S2C and C2S). At first, the entire battery string transfers charge to the battery cell with the lowest voltage ($Cell_1$). Then, the battery cell with the highest voltage releases its charge to

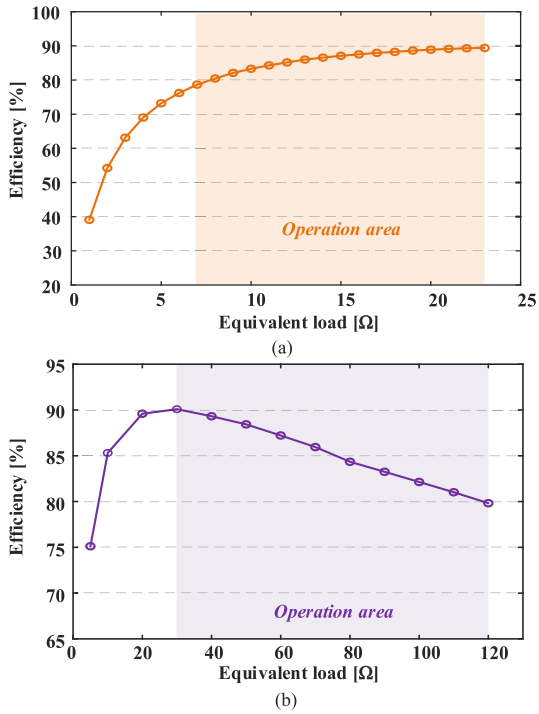

Fig. 17. Experimentally measured conversion efficiency versus equivalent load. (a) S2C mode. (b) C2S mode.

the entire battery string. In Fig. 16(a), the initial voltages of series-connected batteries are 3.914, 3.814, 3.811, and 3.723 V, respectively. As shown, the equalization circuit reduces the voltage difference from 191 to 9 mV in 3450 s. As shown in Fig. 17(a), the conversion efficiency in S2C mode is measured as 89.4%. In Fig. 16(b), the initial voltages of series-connected batteries are 3.818, 3.735, 3.732, and 3.632 V, respectively. The equalization circuit reduces the voltage difference from 186 to 15 mV in 3610 s. As shown in Fig. 17(b), the conversion efficiency in the C2S mode is measured as 90.1%.

VI. Comparison With Existing Battery Equalizers

A systematic comparison of the proposed scheme with traditional equalization systems is given in Tables II and III. Table II compares main components count, and voltage stress of switches, including MOSFETS, drivers, diodes, inductors, capacitors, transformers, and selection switches. Table III compares the performance of these equalizers, including "energy flow types," "frequency," "open-loop current control," "constant speed," "current sensor," "efficiency," and "size & weight." Among them, open-loop current control algorithm is implemented that is denoted by "Yes (Y)," whereas "No (N)" is not used. Similarly, constant speed and current sensor can be denoted by binary criteria (Yes or No).

A. Component Number Comparison

Compared with other unidirectional equalizers, the proposed equalizer only adds two active switches to achieve a bidirectional charge transfer path. Moreover, the L2C3 converter has

TABLE II
COMPARISON OF DIFFERENT EQUALIZERS IN TERMS OF THE COMPONENT NUMBER

Topologies	Switches and drivers	SW stress	Diodes	Capacitors	Inductors	Transformers (turns ratio)	Selection switches
Half-bridge converter [29]	2	NV_c	$2N$	$2(N+1)$	$2N$	1(12:15)	0
LCC converter [22]	2	NV_c	2	2	1	1(14:7)	$2N$
Flyback converter [21]	$2(N-1)$	NV_c	$2N-1$	0	0	1(7:21)	0
Multi winding transformer [20]	N	V_c	$\frac{N}{2}$	0	0	$\frac{N}{2}$(1:1)	0
Class-D and multi active-bridge [17]	$2N+\frac{N}{2}$	$4V_c$	0	N	$2N$	$N(1)+\frac{N}{4}(3)$	0
LLC and buck-boost [16]	$6m+2$	NV_c	2	2	3m	1(3)	$m+5$
Cascade DAB [30]	8	NV_c	0	2	2	$1(5:20)$	$N+1$
Quasi resonant [31]	8	NV_c	2	2	1	$1(5:30)$	$N+1$
Capacitively isolated DAB [32]	$N+1$	$(N/m)V_c$	0	$4m-2$	$4m-1$	0	$m(N+2)$
Bidirectional flyback [37]	2	NV_c	2	0	0	$2(80:35)$	$2N$
This work	4	NV_c	0	3	1	$1(12:12)$	$2N$

The cell voltage is assumed equal to V_c. m and N is the number of cell modules and single cells, respectively.

TABLE III
COMPARISON OF DIFFERENT EQUALIZERS IN TERMS OF THE BALANCING PERFORMANCES

Topologies	Energy flow types	Frequency (Hz)	Open-loop current control	Constant speed	Current sensor	Efficiency (%)	Size and weight
Half-bridge converter [29]	S2C	200 k	N	N	N	≈ 88	small
LCC converter [22]	S2C	200 k	Y	Y	N	88.1	mid
Flyback converter [21]	C2S	25 k and 37.5 k and 75 k	N	N	N	$70 \sim 88$	small
Multi winding transformer [20]	C2S	10 k	N	N	N	–	large
Class-D and multi active-bridge [17]	HME	200 k and 13.56 M	N	N	Y	74 and 93	small
LLC and buck-boost [16]	HME	100 k and 200 k	N	Y	Y	92.48 and 93.5	large
Cascade DAB [30]	S2C/C2S	40 k	N	Y	Y	85.1 and 84.3	large
Quasi resonant [31]	S2C/C2S	20 k	N	Y	Y	84.2 and 83.4	small
Capacitively isolated DAB [32]	S2C/C2S	100 k	N	N	N	84 and 96	large
Bidirectional flyback [37]	S2C/C2S	40 k	N	N	N	85 and 92	mid
This work	S2C/C2S	200 k	Y	Y	N	89.4 and 90.1	small

Y:Yes, N:No.

fewer MOSFETS than DAB converter solutions [30], [32]. Due to the utilization of multiplexer, most bidirectional equalization systems need to connect the battery string to the input of the converter. Therefore, the voltage stress of MOSFETS is NV_c. Both the primary and secondary sides of the converter use the active bridge, and the rectifier diodes are removed. Therefore, synchronous rectification can be implemented to improve efficiency. Compared with the traditional LCC converter [22], L2C3 converter has an extra capacitor, which realizes bidirectional charge transfer. In addition, the secondary side leakage inductance of the transformer is used as the resonant component, which can reduce a magnetic element and reduce the weight and volume of the circuit.

Fig. 18 shows the cost comparison of the balancing circuits. To estimate the cost of the equalizers fairly, the unit cost of the system should be shared equally among each cell (Cost $=$ C_{total}/N). As shown, the cost of the proposed architecture is one of the lowest in all bidirectional equalizers.

B. Balancing Performance Comparison

"Energy flow types" is determined by the equalization structures. The HMEs and bidirectional equalizers have more flexible energy flow. However, HMEs usually utilize multilevel structures to increase energy path with increased component count and control complexity. Among all bidirectional equalizers, the proposed L2C3 converter has the highest switching frequency, which helps to improve the power density. Thus, the equalization system has advantages in size. On the other hand, the balancing circuit uses open-loop control to reduce control complexity. The constant balancing current and speed are achieved. This facilitates a simple estimation of battery state, which helps the controller make judgment on the equalization time. The equalizer presented in [30] and [31] realizes constant balancing speed. However, current sensors are required, which increases the circuit cost and complexity.

In [22], the LCC-based equalizer realizes constant current without current sensors. However, the circuit can only realize

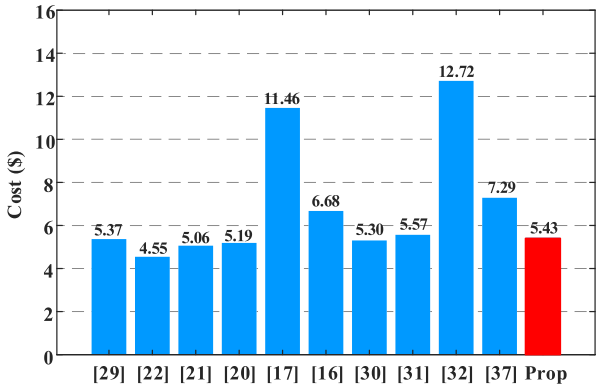

Fig. 18. Cost comparison of unit cost between circuits in the proposed architecture and other active balancing circuits. Component cost per unit ($): MOSFET (0.27–0.78), MOSFET Driver IC (1.8), GaN (4.15), Diode (1.06), Capacitor (0.2), Inductor (0.6), Transformer Core (0.9), winding (0.2), Relay (0.6) [16], [38].

the unidirectional energy flow. The proposed equalizer achieves good efficiency in S2C and C2S mode as all the MOSFETS can achieve ZVS turning-ON and synchronous rectification.

In summary, compared with existing methods, the L2C3-based equalizer operates at fixed-frequency to ensure constant current balancing and maintain low control complexity. Meanwhile, the circuit size is small, and the cost is one of the lowest in all referred equalizers. Therefore, the proposed L2C3-based equalizer exhibits a satisfactory solution for battery equalization systems.

VII. Conclusion

This article proposes a novel bidirectional L2C3 converter and applies it to the battery equalization system, combining the advantages of both S2C and C2S structures. The secondary leakage inductor of the transformer is used as the resonant inductor to reduce the weight and volume of the system. Both primary and secondary sides of the converter adopt an active bridge, which can realize synchronous rectification to mitigate the conduction loss. Compared with existing bidirectional solutions, the proposed equalizer is featured fewer components, smaller size, and lower cost. Furthermore, the proposed converter realizes bidirectional constant current output at fixed switching frequency, which reduces the control complexity. Meanwhile, constant current ensures the simplicity of battery state estimate and stable speed. Moreover, ZVS operations are achieved in both S2C and C2S modes, which reduces the switching loss. A prototype with 196.0 and 204.1 kHz bidirectional equalizer for four battery cells is designed and tested to verify the analysis and the system performance. The measured peak balancing efficiency is 89.4 % in S2C mode and 90.1 % in C2S mode.

References

[1] M. A. Hannan et al., "Toward enhanced state of charge estimation of Lithium-ion batteries using optimized machine learning techniques," *Sci. Rep.*, vol. 10, no. 1, pp. 1–15, Mar. 2020.

[2] M. A. Hannan et al., "SOC estimation of Li-ion batteries with learning rate-optimized deep fully convolutional network," *IEEE Trans. Power Electron.*, vol. 36, no. 7, pp. 7349–7353, Jul. 2021.

[3] F. Feng, X. Hu, J. Liu, X. Lin, and B. Liu, "A review of equalization strategies for series battery packs: Variables, objectives, and algorithms," *Renewable Sustain. Energy Rev.*, vol. 116, 2019, Art. no. 109464.

[4] N. Ghaeminezhad, Q. Ouyang, X. Hu, G. Xu, and Z. Wang, "Active cell equalization topologies analysis for battery packs: A systematic review," *IEEE Trans. Power Electron.*, vol. 36, no. 8, pp. 9119–9135, Aug. 2021.

[5] F. Peng, H. Wang, and L. Yu, "Analysis and design considerations of efficiency enhanced hierarchical battery equalizer based on bipolar CCM buck–boost units," *IEEE Trans. Ind. Appl.*, vol. 55, no. 4, pp. 4053–4063, Jul./Aug. 2019.

[6] S. Wali et al., "Grid-connected lithium-ion battery energy storage system: A bibliometric analysis for emerging future directions," *J. Cleaner Prod.*, vol. 334, Feb. 2022, Art. no. 130272.

[7] S. B. Wali et al., "Battery storage systems integrated renewable energy sources: A biblio metric analysis towards future directions," *J. Energy Storage*, vol. 35, Mar. 2021, Art. no. 102296.

[8] M. Hannan et al., "Battery energy-storage system: A review of technologies, optimization objectives, constraints, approaches, and outstanding issues," *J. Energy Storage*, vol. 42, Oct. 2021, Art. no. 103023.

[9] J. Liu, P. Gao, W. Liao, and J. Zeng, "An integrated energy storage system with voltage balancing based on switched-capacitor reutilization techniques," *IEEE Trans. Veh. Technol.*, vol. 69, no. 8, pp. 8356–8366, Aug. 2020.

[10] Y. Shang, C. Zhang, N. Cui, and C. C. Mi, "A delta-structured switched-capacitor equalizer for series-connected battery strings," *IEEE Trans. Power Electron.*, vol. 34, no. 1, pp. 452–461, Jan. 2019.

[11] Y. Chen, X. Liu, Y. Cui, J. Zou, and S. Yang, "A multiwinding transformer cell-to-cell active equalization method for Lithium-ion batteries with reduced number of driving circuits," *IEEE Trans. Power Electron.*, vol. 31, no. 7, pp. 4916–4929, Jul. 2016.

[12] E. Chatzinikolaou and D. J. Rogers, "Performance evaluation of duty cycle balancing in power electronics enhanced battery packs compared to conventional energy redistribution balancing," *IEEE Trans. Power Electron.*, vol. 33, no. 11, pp. 9142–9153, Nov. 2018.

[13] Y. Lu, Z. Wei, and H. Wang, "A bidirectional cell-to-buffer battery equalizer at boundary conduction mode with constant on-time control," in *Proc. IEEE Energy Convers. Congr. Expo.*, 2021, pp. 1405–1412.

[14] M. Evzelman, M. M. U. Rehman, K. Hathaway, R. Zane, D. Costinett, and D. Maksimovic, "Active balancing system for electric vehicles with incorporated low-voltage bus," *IEEE Trans. Power Electron.*, vol. 31, no. 11, pp. 7887–7895, Nov. 2016.

[15] L. Liu et al., "A low-cost multiwinding transformer balancing topology for retired series-connected battery string," *IEEE Trans. Power Electron.*, vol. 36, no. 5, pp. 4931–4936, May 2021.

[16] F. Peng, H. Wang, and Z. Wei, "An LLC-based highly efficient S2M and C2C hybrid hierarchical battery equalizer," *IEEE Trans. Power Electron.*, vol. 35, no. 6, pp. 5928–5937, Jun. 2020.

[17] M. Liu, Y. Chen, Y. Elasser, and M. Chen, "Dual frequency hierarchical modular multilayer battery balancer architecture," *IEEE Trans. Power Electron.*, vol. 36, no. 3, pp. 3099–3110, Mar. 2021.

[18] Z. Zhang, H. Gui, D. J. Gu, Y. Yang, and X. Ren, "A hierarchical active balancing architecture for lithium-ion batteries," *IEEE Trans. Power Electron.*, vol. 32, no. 4, pp. 2757–2768, Apr. 2017.

[19] S. Li, C. C. Mi, and M. Zhang, "A high-efficiency active battery-balancing circuit using multiwinding transformer," *IEEE Trans. Ind. Appl.*, vol. 49, no. 1, pp. 198–207, Jan./Feb. 2013.

[20] C.-S. Lim, K.-J. Lee, N.-J. Ku, D.-S. Hyun, and R.-Y. Kim, "A modularized equalization method based on magnetizing energy for a series-connected lithium-ion battery string," *IEEE Trans. Power Electron.*, vol. 29, no. 4, pp. 1791–1799, Apr. 2014.

[21] A. M. Imtiaz and F. H. Khan, "Time shared flyback converter' based regenerative cell balancing technique for series connected Li-ion battery strings," *IEEE Trans. Power Electron.*, vol. 28, no. 12, pp. 5960–5975, Dec. 2013.

[22] Z. Wei, F. Peng, and H. Wang, "An LCC-based string-to-cell battery equalizer with simplified constant current control," *IEEE Trans. Power Electron.*, vol. 37, no. 2, pp. 1816–1827, Feb. 2022.

[23] M. Arias, J. Sebastián, M. M. Hernando, U. Viscarret, and I. Gil, "Practical application of the wave-trap concept in battery–cell equalizers," *IEEE Trans. Power Electron.*, vol. 30, no. 10, pp. 5616–5631, Oct. 2015.

[24] C. Hua and Y. Fang, "A charge equalizer with a combination of APWM and PFM control based on a modified half-bridge converter," *IEEE Trans. Power Electron.*, vol. 31, no. 4, pp. 2970–2979, Apr. 2016.

[25] M. M. Hoque, M. A. Hannan, A. Mohamed, and A. Ayob, "Battery charge equalization controller in electric vehicle applications: A review," *Renewable Sustain. Energy Rev.*, vol. 75, pp. 1363–1385, 2017.
[26] Z. Gong et al., "Distributed control of active cell balancing and low-voltage bus regulation in electric vehicles using hierarchical model-predictive control," *IEEE Trans. Ind. Electron.*, vol. 67, no. 12, pp. 10464–10473, Dec. 2020.
[27] J. Carter, Z. Fan, and J. Cao, "Cell equalisation circuits: A review," *J. Power Sources*, vol. 448, pp. 227–489, 2020.
[28] C. Zhang, Y. Shang, Z. Li, and N. Cui, "An interleaved equalization architecture with self-learning fuzzy logic control for series-connected battery strings," *IEEE Trans. Veh. Technol.*, vol. 66, no. 12, pp. 10923–10934, Dec. 2017.
[29] M. Uno and A. Kukita, "String-to-battery voltage equalizer based on a half-bridge converter with multistacked current doublers for series-connected batteries," *IEEE Trans. Power Electron.*, vol. 34, no. 2, pp. 1286–1298, Feb. 2019.
[30] X. Qi, Y. Wang, and M. Fang, "An integrated cascade structure-based isolated bidirectional DC–DC converter for battery charge equalization," *IEEE Trans. Power Electron.*, vol. 35, no. 11, pp. 12003–12021, Nov. 2020.
[31] J. Lu, Y. Wang, and X. Li, "Isolated bidirectional DC–DC converter with quasi-resonant zero-voltage switching for battery charge equalization," *IEEE Trans. Power Electron.*, vol. 34, no. 5, pp. 4388–4406, May 2019.
[32] M. Uno and K. Yoshino, "Modular equalization system using dual phase-shift-controlled capacitively isolated dual active bridge converters to equalize cells and modules in series-connected Lithium-ion batteries," *IEEE Trans. Power Electron.*, vol. 36, no. 3, pp. 2983–2995, Mar. 2021.
[33] S. Mukherjee, A. Sepahvand, and D. Maksimović, "High-frequency LC3L resonant DC-DC converter for automotive LED driver applications," in *Proc. IEEE Appl. Power Electron. Conf. Expo.*, 2018, pp. 797–802.
[34] A. J. Gilbert, D. A. Stone, C. M. Bingham, and M. P. Foster, "Design of an LCC current-output resonant converter for use as a constant current source," in *Proc. Eur. Conf. Power Electron. Appl.*, 2007, pp. 1–6.
[35] R. L. Steigerwald, "A comparison of half-bridge resonant converter," *IEEE Trans. Power Electron.*, vol. 3, no. 2, pp. 174–182, Apr. 1988.
[36] M. Zhou, D. Shu, and H. Wang, "An H5-Bridge-based laddered CLLC DCX with variable DC link for PEV charging applications," *IEEE Trans. Power Electron.*, vol. 37, no. 4, pp. 4249–4260, Apr. 2022.
[37] M. A. Hannan et al., "Lithium-ion battery charge equalization algorithm for electric vehicle applications," *IEEE Trans. Ind. Appl.*, vol. 53, no. 3, pp. 2541–2549, May/Jun. 2017.
[38] "Digikey electronics electronic components distributor," Accessed on: Jun. 20, 2022. [Online]. Available: https://www.digikey.com

Zhengqi Wei (Student Member) received the B.S. degree in electronic information science and technology from Shaanxi Normal University, Xi'an, China, in 2019, and the M.S. degrees from the School of Information Science and Technology, ShanghaiTech University, Shanghai, China, in 2022. He is currently working toward the Ph.D. degree in electronic engineering with the City University of Hong Kong, Hong Kong.

His research interests include battery management system and battery equalization.

Haoyu Wang (Senior Member) received the bachelor's degree with distinguished honor in electrical engineering from Zhejiang University, Hangzhou, China, and the master's and Ph.D. degrees from the University of Maryland, College Park, MD, USA, both in electrical engineering.

In September 2014, he was with the School of Information Science and Technology, where he is currently an Associate Professor with tenure. His research interests include power electronics, plug-in electric and hybrid electric vehicles, the applications of wide-bandgap semiconductors, renewable energy harvesting, and power management integrated circuits.

Dr. Wang is an Associate Editor for the IEEE TRANSACTIONS ON INDUSTRIAL ELECTRONICS, IEEE TRANSACTIONS ON TRANSPORTATION ELECTRIFICATION, and CPSS TRANSACTIONS ON POWER ELECTRONICS AND APPLICATIONS.

Yiqing Lu received the B.S degree in information engineering from Zhejiang University, Hangzhou, China, in 2020. He is currently working toward the Ph.D. degree with the School of Information Science and Technology, ShanghaiTech University, Shanghai, China.

His research interests include battery management system and battery modeling.

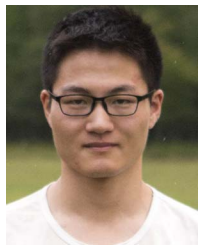

Dongdong Shu received the B.S. degree in automation from Northwestern Polytechnic University, Xi'an, China, in 2016. He is currently working toward the Ph.D. degree with the School of Information Science and Technology, ShanghaiTech University, Shanghai, China.

His research interests include ultrawide voltage range LLC converter and bidirectional dc/dc converter.

Guangdong Ning received the B.S. degree in electrical engineering and automation from the Nanjing University of Aeronautics and Astronautics, Nanjing, China, in 2017. He is currently working toward the Ph.D. degree with the School of Information Science and Technology, ShanghaiTech University, Shanghai, China. His research focuses on the modular design of resonant converters.

Minfan Fu (Senior Member) received the B.S., M.S., and Ph.D. degrees in electrical and computer engineering from the University of Michigan-Shanghai Jiao Tong University Joint Institute, Shanghai Jiao Tong University, Shanghai, China, in 2010, 2013, and 2016, respectively.

From 2016 to 2018, he held a postdoctoral position with the Center for Power Electronics Systems, Virginia Polytechnic Institute and State University, Blacksburg, VA, USA. He is currently an Assistant Professor with the School of Information Science and Technology, ShanghaiTech University, Shanghai, China. His research interests include megahertz wireless power transfer, high-frequency power conversion, high-frequency magnetic design, and application of wide-bandgap devices.